Preprint/Prétirage

Removing Unwanted Fluctuations in the AVHRR Thermal Calibration Data Using Robust Techniques

A.P. Trishchenko

Canada Centre for Remote Sensing, Natural Resources Canada
Ottawa, Ontario, Canada
K1A 0Y7
E-mail: trichtch@ccrs.nrcan.gc.ca

ABSTRACT

The study deals with analysis of thermal calibration of the Advanced Very High Resolution Radiometer (AVHRR) aboard National Oceanic and Atmospheric Administration (NOAA) spacecrafts. In particular, the effects caused by various types of contamination or corruption of the thermal calibration data are investigated. These phenomena lead to perturbations of the true signal, referred to here as unwanted fluctuations. They must be removed or corrected to maximum possible extent to reduce the error in the calibrated data. It is shown that methods currenty employed in operational practice at NOAA and the Canada Centre for Remote Sensing (CCRS) frequently fail to remove some of the unwanted fluctuations in calibration data that may lead to biases in brightness temperature excceding 1 K. A complex method for removing unwanted fluctuations in the thermal calibration data specifically designed for the AVHRR radiometers is proposed. The procedure is based on combining robust statistical procedures and Fourier transform filtering techniques. Application of the method is considered for various components of calibration data: temperature sensors, blackbody, and space count, as well as gain in all thermal channels. High Resolution Picture Transmission (HRPT) data and Global Area Coverage (GAC) data are analyzed. Power spectra analysis of the calibration data has been conducted to estimate impact of various frequency harmonics. The method proposed may be useful for the development of calibration techniques for similar radiometers and the future National Polar-Orbiting Operational Environmental Satellite System.

1. Introduction

The Advanced Very High Resolution Radiometer (AVHRR) onboard National Oceanic and Atmospheric Administration (NOAA) satellites is one of the most widely used sensors for remote sensing of the earth atmosphere and surface (Cracknell 1997; Kidwell 1998). Datasets of sea surface temperature (SST), land surface properties, and Normalized Difference Vegetation Index derived from the AVHRR observations are now an integral part of many weather prediction systems. Twenty-one years of AVHRR data are currently archived. Long-term series of the AVHRR-based surface and atmospheric parameters are used in many environmental and climate change studies (Reynolds and Smith 1994; Cihlar et al.1998; Gutman 1999; Peterson et al. 2000; Cihlar et al. 2002b). This demands high accuracy in the radiometric calibration of the AVHRR data.

The AVHRR radiometer has two solar channels: channel 1 (red), channel 2 (near-IR), and three thermal channels: channel 3B (3.7 μm), channel 4 (11, μm), and channel 5 (12 μm). The latest version of the AVHRR radiometer (AVHRR/3) installed onboard *NOAA-15* and *NOAA-16* has an additional channel 3A (1.6 μm) that operates instead of channel 3B on the sunlit part of a satellite orbit. The bandwidth of channel 3B (3.7, μm) makes it sensitive to solar-reflected and thermal radiation. However, because this channel is calibrated in the same way as channels 4 and 5, through the observation of internal blackbody, we consider it as a thermal channel as well.

Since thermal channels are calibrated in-flight, it is often believed that high quality of output data is automatically ensured. However, it is not always the case. The reason is that the satellite data are prone to noise. Distortion of the data may occur during transmission of the signal through the atmosphere. Data may also be contaminated by processes occurring in the instrument, for example, during digital conversion, fluctuations of the instrument thermal state or solar contamination of calibration cycles. These phenomena, which we call unwanted fluctuations, lead to perturbations of the true signal. They must be removed or corrected as much as possible to ensure accurate calibration. This task is achieved by quality control and correction procedures.

Despite the long history of observations and numer-

Published in the Journal of Atmospheric and Oceanic Technology, Volume 19, number 12, 2002
pp. 1939-1954

ous studies on application of the AVHRR thermal data, aspects of the AVHRR data processing related to data quality control and correction of contaminated data still are not addressed properly. This study intends to partially fill this gap based on experience with processing of the AVHRR data using the New Goecoding and Compositing System (GEOCOMP-N) employed at the Canada Centre for Remote Sensing (CCRS) (Adair et al. 2002; Cihlar et al. 2002a) and Global Area Coverage (GAC) data acquired from NOAA Satellite Active Archive (SAA).

Unlike many specialized communication systems (Houghton 2001; Viterbi and Omura 1979), the data transmission link of NOAA satellites does not provide redundancy coding. Therefore, any noise arising during propagation of the radio waves through the atmosphere appears in the satellite data on equal footing with the true signal. This is especially evident at low receiving antenna elevation angles, when the distance to satellite is the largest and the intensity of the radio signal is small (Alexejev et al. 1994). The overall effect of outliers may be quite large even if they are sparse, since their magnitude may differ very much from that of a typical calibration signal. This is especially true for calibration data, which typically are either constant or weakly varying variables.

The errors in data may not necessarily be caused by signal transmission and/or bit decoding. They may also be artefacts emerging as a result of onboard signal transformation or digitization. An example of this kind is shown later and is related to errors in coding of Platinum Resistance Thermometer (PRT) measurements. The PRT data are used in determining temperature of calibration target, as such, this information is of critical importance for accurate thermal calibration.

Another example of unwanted fluctuations in calibration data is so-called solar radiative contamination of calibration cycles (Steyn-Ross et al. 1992; Trishchenko and Li 2001a). These fluctuations appear on certain parts of satellite orbits when geometrical conditions allow solar light to reach the surface of AVHRR's internal calibration target or to contaminate the deep space observations. In these circumstances, the true calibration signal from the internal calibration target (ICT) and deep space signal (SP) is contaminated by external solar radiation. Calibration coefficients computed without correction for solar contamination lead to biased results.

The paper is organized as follows. Section 2 discusses briefly the AVHRR thermal calibration approach, as well as examples and consequences of faulty onboard calibration samples, such as ICT, SP, and PRT counts. Section 3 explains the principles of the robust approach proposed for quality control of AVHRR data and removing unwanted fluctuations in calibration data. Section 4 provides the details and specific parameters recommended for implementation in an operational data processing for various historic and current AVHRR instruments (*NOAA-9* to *NOAA-16*). Section 5 presents recommendations for quality control and correction of the gain (G) and offset (I) radiance calibration coefficients. Section 6 analyzes the effect of time-dependent gain on the calibration of HRPT scenes. Section 7 concludes the paper with a discussion of results and recommendations.

2. AVHRR thermal calibration and impact of unwanted fluctuations

An example of unwanted fluctuations in the AVHRR calibration parameters is illustrated in Fig. 1. It shows the AVHRR/*NOAA-14* calibration data averaged over an entire image (~15-min long) acquired at Prince Albert Satellite Station (PASS) in Saskatchewan, Canada. This is the principal receiving station that supplies AVHRR data for Canada Centre for Remote Sensing. Data presented in Fig. 1 cover period of 4.5 months spanning from the beginning of February to the end of June 2000. GEOCOMP-N system was used to process data (Adair et al. 2002; Cihlar et al. 2002a). The calibration of thermal data employed scene average values for ICT temperature, SP, and ICT counts. The system includes several data quality control procedures to screen out crude errors in image data for each spectral band. These procedures determine scan line average absolute difference between raw counts from adjacent pixels. If the difference is ''abnormally'' high or low it suggests that data are either noisy or lost (filled by blank words).

Despite measures to remove bad image scan lines from analysis, the calibration data for some scenes shown in Fig. 1 are clearly corrupted, even though they represent scene average values for more than 5000 scan lines. Outliers in scene-average calibration data with a magnitude of 5–10 counts are quite usual. Three vertical columns of Fig. 1 correspond to each of the three thermal channels. Horizontal panels show instrument counts for ICT and SP counts, as well as gain G computed according to

$$G^{(i)} = \frac{R^{(i)}_{\mathrm{ICT}}(T_{\mathrm{ICT}}) - R^{(i)}_{\mathrm{SP}}}{C^{(i)}_{\mathrm{ICT}} - C^{(i)}_{\mathrm{SP}}}, \tag{1}$$

where $R^{(i)}_{\mathrm{ICT,SP}}$ is either radiance of blackbody at temperature T_{ICT} in spectral channel (i) or ''effective'' nonzero radiance assigned to space, while $C^{(i)}_{\mathrm{ICT,SP}}$ is a corresponding count (Kidwell 1998). The radiance of a pixel in linear approximation is computed as

$$R^{(i)} = G^{(i)} C^{(i)}_{\mathrm{pix}} + I^{(i)}, \tag{2}$$

where $C^{(i)}_{\mathrm{pix}}$ is the pixel count, and $I^{(i)}$ is the offset in channel (i) defined as

$$I^{(i)} = R^{(i)}_{\mathrm{SP}} - G^{(i)} C^{(i)}_{\mathrm{SP}}. \tag{3}$$

For channels 4 and 5 one needs to apply a nonlinear correction to obtain corrected radiance (Kidwell 1998; Sullivan 1999).

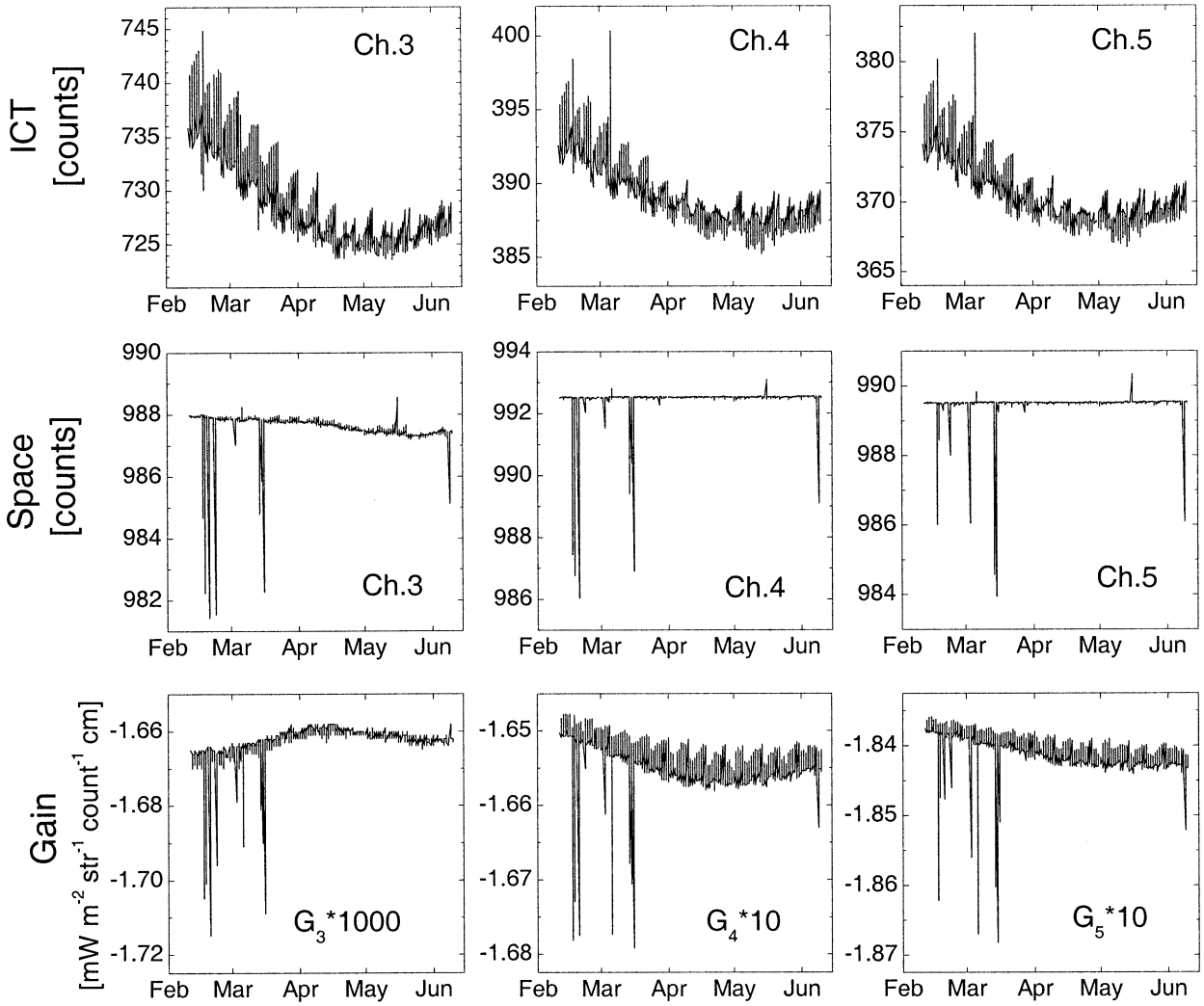

FIG. 1. Scene average calibration parameters for AVHRR HRPT data acquired at Prince Albert Satellite Station (PASS), Saskatchewan, Canada. Data are shown for the AVHRR *NOAA-14*. They cover a period from Feb to Jun 2000. The three columns correspond to channels 3B, 4, and 5. The rows are for ICT, SP, and channel gains $G^{(i)}$. Occasional noisy outliers can be seen.

An example of noiselike fluctuations in the GAC data is given in Fig. 2a. Data were processed at NOAA and acquired through the NOAA SAA. It is quite clear that fluctuations cannot represent the real changes in channel gain, there is no physics behind such behavior. If uncorrected, these fluctuations lead to quite substantial errors (more than 1 K) in pixel brightness temperature. Figure 2b demonstrates the effect of data reception on quality of the HRPT calibration data. Irregularities in the beginning and end of data reception occur due to low signal to noise ratio and loss of hardware synchronization. In this case data words are filled either by ''1'' and ''0'' bits. A large deviation from normal signal may bias significantly calibration coefficients, if it is not properly corrected for.

Figure 3 gives an example of corrupted PRT counts leading to erroneous determination of ICT temperature. There are four PRT detectors designed for monitoring the ICT temperature. Data in Fig. 3 are presented for PRT #3 of the AVHRR onboard *NOAA-9* on 1 November 1988. Many spikes of up to 10 counts ($\sim$0.6 K in temperature) can be observed. They do not represent a real signal, since the thermal state of the massive ICT cannot be changed instantaneously. These spikes, therefore, are artefacts, and they must be removed. Similar fluctuations exist for other PRTs.

The effect of data corruption on pixel brightness temperature depends on which variable is affected. The error ΔT in temperature of internal calibration target T_{ICT} translates directly in the determination of pixel brightness temperature. It is equal to ΔT for scene temperatures close to T_{ICT}, which is approximately in the range of 285–300 K. It decreases to zero for very small radiance values approaching signal level close to the one observed during the deep space observation. The errors in SP and ICT counts have a different impact on the

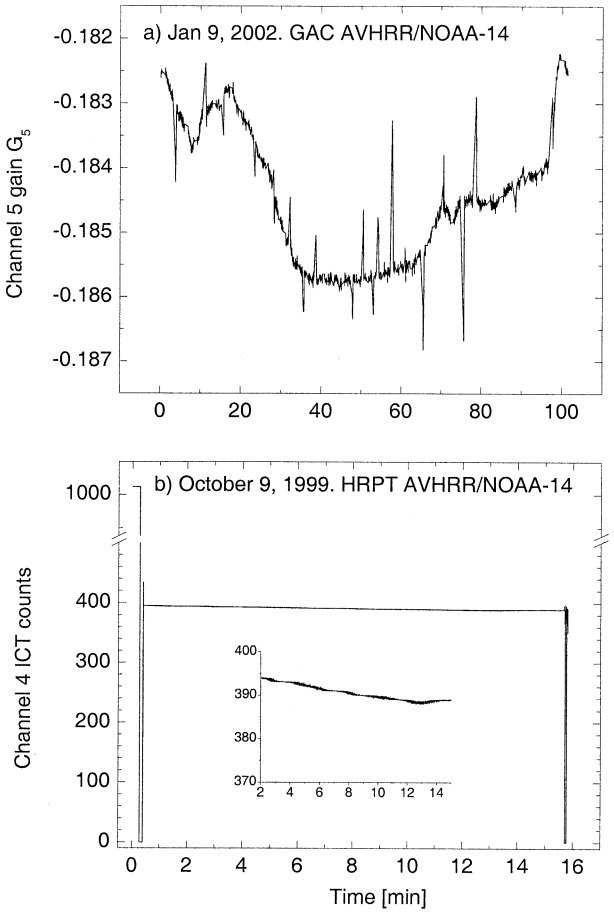

FIG. 2. An example of noisy fluctuations in (a) AVHRR GAC data and (b) HRPT data. Data are for AVHRR/*NOAA-14*. The insertion in the bottom panel shows the signal without outliers.

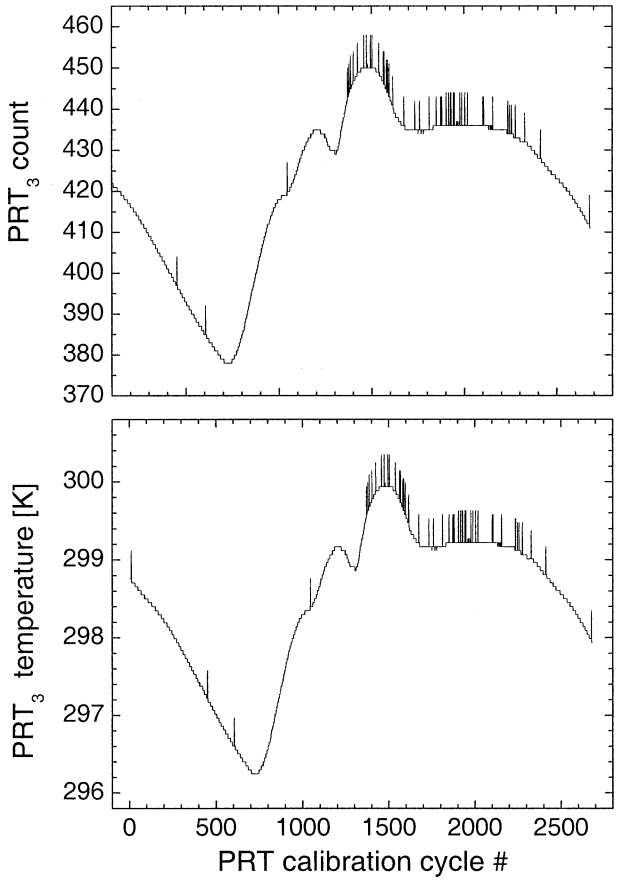

FIG. 3. (top) Outliers in the signal for AVHRR PRT #3 onboard *NOAA-9*. (bottom) Corresponding temperature fluctuations. Data are for 1 Nov 1988.

brightness temperature error. The error, as function of brightness temperature, may be determined from the following expressions

$$\Delta R(T_P)|_{\mathrm{SP}} = \frac{R(T_P) - R_{\mathrm{ICT}}}{C_{\mathrm{ICT}} - C_{\mathrm{SP}}}\Delta C_{\mathrm{SP}}, \tag{4a}$$

$$\Delta R(T_P)|_{\mathrm{ICT}} = -\frac{R(T_P) - R_{\mathrm{SP}}}{C_{\mathrm{ICT}} - C_{\mathrm{SP}}}\Delta C_{\mathrm{ICT}}, \tag{4b}$$

$$\Delta R(T_P)|_{T} = \frac{C(T_P) - C_{\mathrm{SP}}}{C_{\mathrm{ICT}} - C_{\mathrm{SP}}}R'(T_{\mathrm{ICT}})\Delta T_{\mathrm{ICT}}, \tag{4c}$$

where

$$R'(T) = \frac{d}{dT}R(T) = \frac{d}{dT}\left(\frac{c_1\upsilon^3}{\exp\left(\frac{c_2\upsilon}{T^*}\right) - 1}\right). \tag{4d}$$

The above expressions were obtained assuming a linear approximation (2), which provides quite accurate results for the estimation purpose. Symbol $\Delta R(T_P)|_{\mathrm{SP,ICT},T}$ denotes the error in pixel radiance due to error in SP counts, ICT counts, or error in determination of calibration target temperature T_{ICT}. Centroid wavenumber υ used in expression (4d) for Planck's function depends on temperature range. Radiometer specific values for various AVHRRs except AVHRR/3 can be found in (Kidwell 1998). For AVHRR/3, υ is a constant and an ''effective blackbody temperature'' T^* is recommended to use in computations (Goodrum et al. 2000). Error in terms of pixel brightness temperature depends on the magnitude of pixel brightness temperature T_P itself and may be derived by inverting Planck's function

$$\Delta T(T_P) = \frac{\Delta R(T_P)|_{\mathrm{SP,ICT},T}}{R'(T_P)}. \tag{5}$$

The structure of temperature errors due to various factors computed using Eqs. (4a–c) is presented in Fig. 4. It was estimated for typical calibration parameters of AVHRR *NOAA-14* at $T_{\mathrm{ICT}} = 289$ K. Figure 4a shows the errors in brightness temperature due to a fluctuation in space count ($\Delta\mathrm{SP} = 10$). Figure 4b shows the corresponding errors due to a fluctuation in ICT count ($\Delta\mathrm{ICT} = 10$). Figure 4c shows the effect of error in determination of calibration target temperature ($\Delta T_{\mathrm{ICT}} = 1$ K). A deviation of 10 counts is a realistic estimate

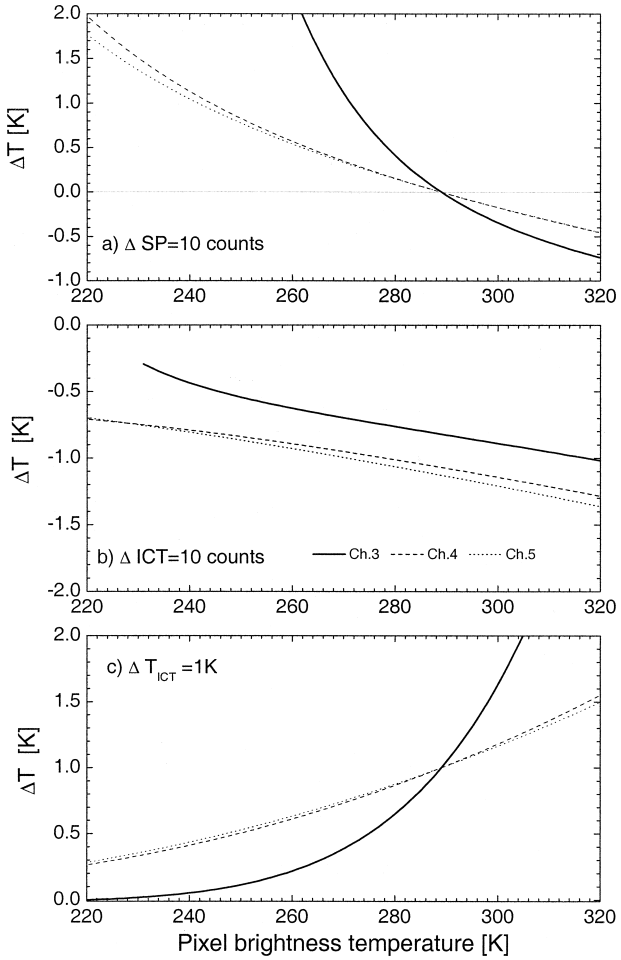

FIG. 4. Errors in pixel brightness temperature due to errors in (a) SP counts, (b) ICT counts, and (c) determination of ICT temperature. The solid line is for channel 3B, dashed line is for channel 4, and dotted line is for channel 5. The temperature of the calibration target was assumed equal to 289 K.

of potential range of variability according to data shown in Fig. 1. Since the calibration is tied to space radiance and ICT radiance, the error in SP count affects mostly pixels with low brightness temperatures, while the error in ICT count affects more the pixels with high brightness temperatures. An error of 10 counts in ICT signal (Fig. 4b) causes an error in brightness temperature for channel 4 and 5 about -1 K and -0.7 K for channel 3 at freezing point ($t = 0$°C). The errors get larger in absolute magnitude when temperature increases. Similar deviation in SP count (Fig. 4a) leads to errors less that ± 0.5 K for channels 4–5 and may reach ± 2 K or more for channel 3. The error in determination of $T_{\rm ICT}$ translates directly into a pixel brightness temperature error for brightness temperature equal to $T_{\rm ICT}$. It decreases by a factor of ~ 2 at $t = 0$°C for channels 4–5 and by factor a of ~ 4 for channel 3. For temperatures greater than $T_{\rm ICT}$, the uncertainty in pixel brightness temperature grows. Curves showing errors for negative increments of ΔSP, ΔICT, and $\Delta T_{\rm ICT}$ are symmetrical relative to x axis to those shown in Fig. 4.

The above values are for the scene average errors with the number of calibration cycles being 5000 or more. In case of a smaller number of samples, the magnitude of errors may be higher, since it is usually inversely proportional to sample size. Though in general the quality of data reception is very high, one can see noise/spikes in the data series, which emphasizes the importance of data quality control and correction procedures. We estimate that on average typically about 1%–2% of monthly scenes may be affected by random noise with a bias close to or greater than 1 K. In the case of problems with satellite transmitters, as experienced in September–October 2001 for *NOAA-16*, and data reception by smaller receiving antennas, data error rates may be much higher.

Another example of unwanted fluctuations in the calibration data is a solar radiative contamination described by Steyn-Ross et al. (1992) and analyzed by Trishchenko and Li (2001a). This sort of error occurs due to direct illumination of the ICT and/or contamination of deep space observations by sunlight. The effect is observed as strong short-term variation of the instrument gain and offset lasting a few minutes. Possible contamination of SP counts affects the channel 3 calibration mainly, since IR channels 4 and 5 are not sensitive to shortwave solar radiation. Solar blackbody contamination affects all thermal channels, since it heats up the ICT surface and causes mismatch between the PRT-measured temperature and the effective temperature of radiation emitted by the ICT surface. Therefore, consequences of this effect are similar to ones presented in Fig. 4c that describes the error in the ICT temperature. In the case of solar contamination of the SP signal, the effect is similar to the one presented in Fig. 4a (noise in SP counts), but may be much higher in magnitude. The effect of solar blackbody contamination is observed also in Figs. 2a and 3 as smooth peaks with a duration of a few minutes.

3. Need for robust methods of error detection

In this section we describe first some basic properties of the AVHRR calibration system and then discuss our approach to data processing and error correction. The AVHRR thermal calibration data are usually smooth and slowly varying functions of time. They typically oscillate with the dominant period equal to the satellite orbital period. Higher-frequency harmonics are also possible due to asymmetry in the distribution of sunlit (heating) and dark (cooling) parts of the spacecraft orbit and due to AVHRR's internal thermal processes. The strongest irregularities occur around the terminator crossing points and during solar contamination events. Variations in gain and offset are relatively smaller in magnitude than variations observed in the ICT and PRT calibration data. The gain and offset represent the internal property

TABLE 1. Interval of single orbit average counts for SPACE and ICT signal for various AVHRR radiometers. Values in parenthesis are data range.

Platform	Period	Type	Channel 3B (counts)	Channel 4 (counts)	Channel 5 (counts)
NOAA-9	1985–88	SP	992–997 (5)	987–989 (2)	993–994 (1)
		ICT	560–739 (179)	311–383 (72)	341–415 (74)
NOAA-11	1988–94	SP	989–991 (2)	993–994 (1)	996–997 (1)
		ICT	670–758 (88)	425–460 (35)	358–408 (50)
NOAA-12	1991–98	SP	992–995 (3)	993–996 (3)	998–1000 (2)
		ICT	625–740 (115)	325–392 (67)	320–388 (68)
NOAA-14	1995–2000	SP	986–989 (3)	992–993 (1)	988–990 (2)
		ICT	718–752 (34)	383–405 (22)	364–386 (22)
NOAA-15	1999–2001	SP	988–990 (2)	988–990 (2)	988–989 (1)
		ICT	635–815 (180)	408–454 (46)	381–427 (46)
NOAA-16	2001	SP	990–991 (1)	991–992 (1)	994–995 (1)
		ICT	850–854 (4)	455–459 (4)	429–434 (5)

of the measurement system, which is designed to be invariant under a wide range of conditions. To make the system more stable to external thermal forcing, the entire detector system is maintained under constant low temperature (107 K) by special radiant coolant subsystem (Cracknell 1997). Nevertheless, gain and offset calibration coefficients manifest a periodic orbital type of oscillation. The question ''are they real or not'' is beyond the scope of this study, since it cannot be answered based solely on in-flight calibration measurements. Nevertheless, some types of variation can be reliably classified as errors based on physics and statistics of the calibration observations.

The AVHRR thermal calibration system is designed in such a way that the SP counts, corresponding to background radiation level (zero level), tend to be maintained at almost constant levels (electronically clamped every scan line). Typical single orbit average SP and ICT values are presented in Table 1 for various AVHRRs onboard *NOAA-9, -11, -12, -14, -15,* and *-16* over their lifetime. Normally, the SP signal variations are quite small, remaining within a few counts for all thermal channels. For the data shown in Table 1, maximum spread between SP counts is five counts for *NOAA-9* over a 7-yr period. The other radiometers exhibit even smaller variations of 1–3 counts. On top of these variations we have to add the amplitude of variation within a single orbit, which is typically of the same magnitude as the range shown in Table 1 or smaller.

In contrast to SP data, the variability of the ICT counts may be quite significant—up to 100 counts or more. This happens mostly due to a change in ICT temperature that changes in synergy with intermittent heating and cooling cycles along the orbit. Some contribution occurs also due to a variation of instrument calibration properties (gain and offset). The PRT data vary substantially but in synergy with ICT data.

The signal representing ICT and PRT calibration data is nonstationary (time-dependent). Noise contamination may cause outliers with very large amplitude. Therefore, the standard quality control procedures based on analysis of statistical distribution (see, e.g., Eskridge et al. 1995), are not always efficient. Instead, some sort of robust techniques adopted for analysis of time series with outliers is required (Barnett and Lewis 1994; Martin 1981; Rousseeuw and Leroy 1987).

Our approach to removing the unwanted fluctuation in the AVHRR thermal calibration data consists of three steps: i) a robust estimation of calibration data to remove single outliers/noise in the data series and bound the calibration signal within narrow limits; ii) application of a Fourier transform filtering technique to further reduce noise in the calibration data that passed through the first step; iii) production of data quality flags for suspicious data, replacement of suspicious input data by results of the filtering process and repeating steps ii) and iii) until the convergence (no further improvement) criterion is achieved. Convergence usually is achieved after the second or third iteration.

4. Removing unwanted fluctuations in the calibration data

a. Robust analysis of calibration samples

Although the AVHRR data do not have redundancy in terms of error correction information, they nevertheless contain certain redundancy in data content. For example, every scan line contains 10 calibration samples of SP and ICT counts and 3 samples of PRT counts. Also, it is very reasonable to expect quite smooth and slowly changing calibration sample data in time. Analysis suggests that one can assume the statistical distribution of calibration samples to be stationary, unimodal, and symmetric over a duration of a few calibration cycles. This information may be employed to remove or minimize the effect of corrupted data. The most effective way consists of applying a robust technique over several scan lines as a replacement to the traditional averaging technique. This enables obtaining the most reliable estimation of ICT, SP, and PRT counts, which is resistant to large outliers. There are small differences in application of the approach for HRPT and GAC data due to differences in data sampling rates.

What we suggest is based on the idea of a statistical median approach, that is, selection of the central data point in the sorted array. We slightly modify this approach to introduce more continuity in the calibration data. To get robust estimate of SP and ICT values we suggest analyzing m consecutive samples, that is, $m \times 10$ elements of data. Selection of a suitable number m for the HRPT and GAC data and various calibration parameters is discussed later. We sort the $m \times 10$ elements in increasing order. Then, we keep 10 central elements only and produce the weighted average of these 10 elements as a replacement for the simple average of the original data. A weighting function is chosen to provide a larger weight to the elements located closer to the median value. This, the weighted average is computed as

$$y = \left(\sum_i w_i y_i\right) \Big/ \left(\sum_i w_i\right). \tag{6}$$

For example, one can choose the weighting function values $w_i = \{1, 2, 3, 4, 5, 5, 4, 3, 2, 1\}$ for i ranging from 1 to 10. Such chosen weighting factors have no rigorous justification. An alternative choice is possible, however, by trying several reasonable approaches, we found its effect generally quite negligible.

We suggest a similar scheme for PRT data: analyzing several (n) consecutive data samples for each PRT sensor. There are three PRT counts in each scan line calibration sample. We analyze a group of $n \times 3$ elements, sort them in increasing order, keep three central elements and produce a weighted average [Eq. (6)] with weights $w_i = \{1, 2, 1\}$ for i ranging from 1 to 3. Data for an individual PRT sensor are not available for every AVHRR scan line, therefore the numbers n for PRT data and m for ICT and SP data may be different. These numbers differ also between GAC and HRPT data. The sample data for each individual PRT sensor are included in every fifth line, therefore n consecutive samples correspond to the time interval $5/6n$ s for HRPT data, and $(0.5)(5)n$ s for GAC data, given that the AVHRR sampling rate is six scan lines per second, and only every third scan line is recorded for GAC data. The corresponding intervals for ICT and SP calibration data are $m/6$ s for HRPT and $0.5m$ s for GAC data. To apply this approach on an equal basis for HRPT and GAC data and for various calibration parameters, we select an elementary time interval of data sampling for robust estimation equal to 12.5 s. This interval is deemed to be short enough to satisfy our requirements for stationary, unimodal, and symmetric data distribution. With this choice, our numbers of data samples are $n = 5$ for PRT data in GAC format, $n = 15$ for PRT data in HRPT format, $m = 25$ for ICT and SP data GAC format, $m = 75$ for ICT and SP data in HRPT format.

An example of results using the proposed robust approach is shown in Fig. 5 for PRT data (top), SP (center) and ICT (bottom) counts for *NOAA-9*. We choose the same GAC data as in Figure 3. To emphasize the improvement achieved by robust estimation, we plotted results obtained by simple averaging and the robust technique using shifted y axes. Much improvement is observed when applying the robust technique. Robust estimation removes most corrupted PRT samples. A remarkable effect is observed for channel 4 SP data where the robust approach refined the calibration data to a nearly constant value. Similar improvement is observed for ICT data shown in the bottom panel of Fig. 5. Overall noise was reduced. Corrupted data for calibration cycles between 2100 and 2200 were completely corrected.

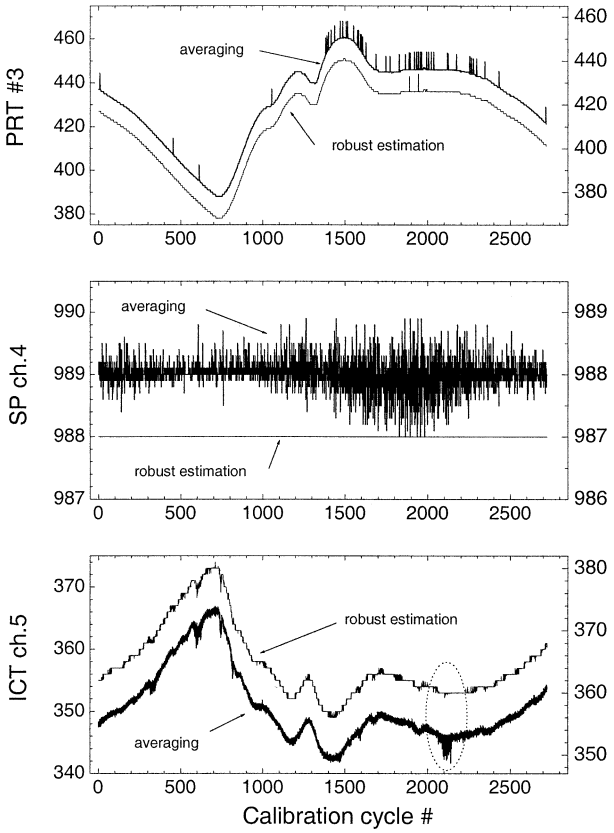

FIG. 5. Scan-line average calibration data for averaging method and robust median estimation. (top) PRT data, (middle) SP data, (bottom) ICT data. Data are given for AVHRR *NOAA-9* on 1 Nov 1988.

The proposed approach cannot remove significant errors that last over 12.5 s. This may happen in the case of very severe interference during the data reception. To cover this rare case with outliers of large magnitude, we apply a threshold technique, which detects data beyond the potential limits of variability. Values falling beyond these limits are flagged as suspicious and replaced by linear interpolation of two adjacent good values.

b. Determination of potential limits

Determination of potential limits for various calibration components depends on the nature of the compo-

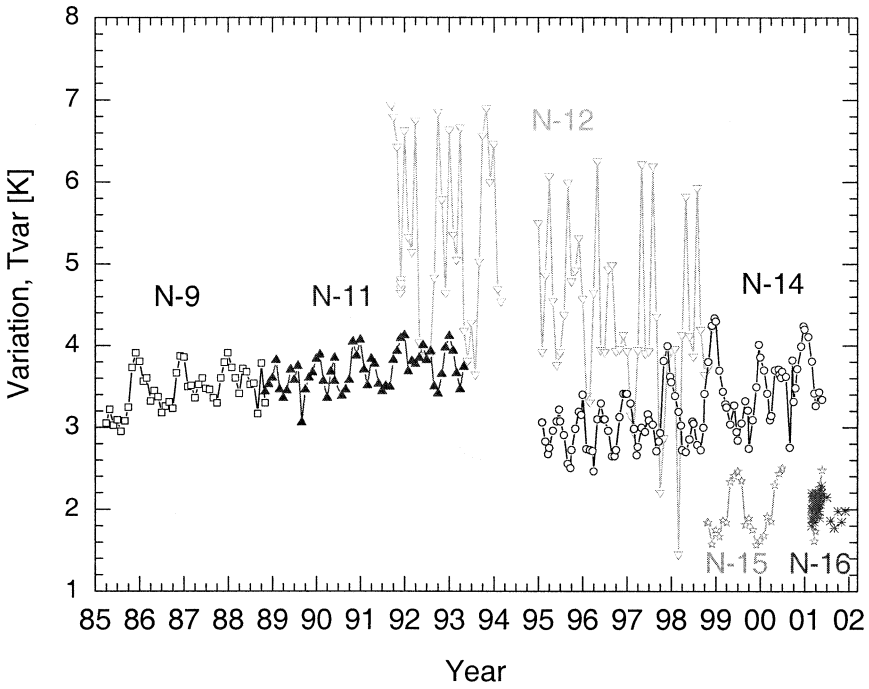

FIG. 6. Amplitude of the ICT temperature variation $T_{var} = T_{max} - T_{min}$ within one orbit for various AVHRR radiometers onboard *NOAA-9* to *-16.*

nent. The application also depends whether it is GAC or HRPT data. In the latter case, the potential range of variability is smaller.

1) SPACE COUNTS

The SP data provide the simplest case. The SP data sequence closely resembles a stationary process with quite a narrow range of variability. First, we suggest computing the grand average for an entire sample (HRPT scene or GAC orbit) processed as described above. Since it is still possible that large errors are present, to compute a grand average, we apply a variant of the robust procedure, which is resistant to large outliers. A grand average is computed for the trimmed dataset where the largest and smallest 5% of the data points are removed. Altogether, we remove 10% of the data with the reasonable assumption that there are less than 10% large outliers in the data. Then, we apply limits of ± 3 counts for channels 4 and 5 and of ± 10 counts for channel 3 around the corresponding grand averages to flag values that are below and above these limits as suspicious. Suspicious values are then replaced by linear interpolation between the two adjacent good data points. The bounding limits for outlier removal are the same for the HRPT and GAC SP data.

2) PRT COUNTS

The assessment of potential limits for PRT counts also employs the robust computation of grand averages for each PRT sensor, based on a trimmed dataset. The limits of potential variability are deduced from a long-term analysis of the ICT temperature for several AVHRR radiometers. Figure 6 shows the maximum variation of ICT temperature $T_{var} = T_{max} - T_{min}$ within a single orbit for the AVHRR radiometers onboard *NOAA-9* to *NOAA-16.* A maximum range of $\sim$7 K is observed for *NOAA-12.* For all other AVHRR radiometers, the range is typically smaller that 5 K. For the new AVHRR/3 radiometers onboard *NOAA-15* and *-16,* the temperature variability within one orbit is less that 3 K. Thus, for the GAC data one can safely impose a limit ± 4 K for AVHRR/*NOAA-12* and ± 2.5 K for all other AVHRR's presented in Fig. 6. For example, the variation of ± 2.5 K around 288 K as the average ICT temperature for AVHRR/*NOAA-14* corresponds to an interval between 172 and 270 counts, that is, covers a range of $\sim$100 counts. The corresponding limits we suggest for the HRPT data are ± 4 K for AVHRR *NOAA-12* and ± 1.5 K for all other radiometers. These limits are applied for every individual PRT sensor. Values that fall outside of the imposed limits are flagged as suspicious and replaced by linear interpolation of adjacent good values.

3) ICT COUNTS

The measurements of blackbody depend on the instrument gain and offset as well as on the ICT temperature. We propose the determination of the potential range for ICT counts based on Eqs. (1)–(3) and robust

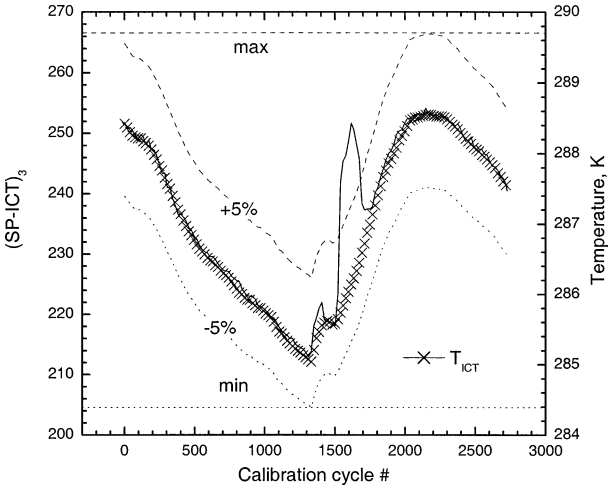

FIG. 7. Determination of bounds for ICT calibration data.

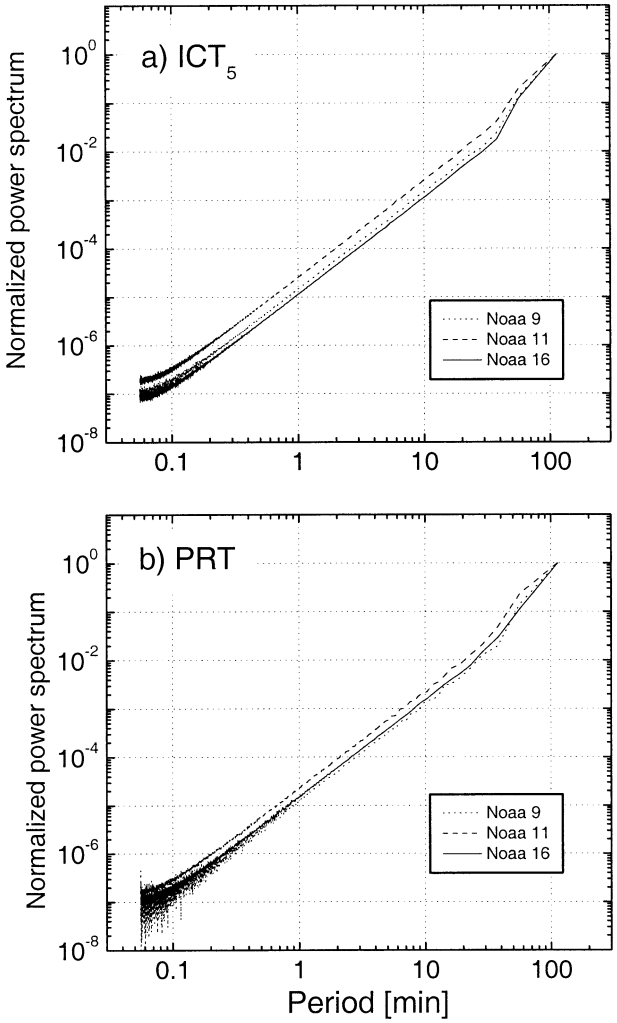

FIG. 8. Examples of power spectrum analysis for ICT and PRT data of AVHRR onboard *NOAA-9, -11, -16.*

estimation of average gain. The robust grand average of ICT signal is again determined by trimming the largest and lowest 5% of ICT data and producing an average for the remaining data points. The average value of gain is then computed according to Eq. (1) with the average ICT temperature determined from available PRT data. We then determine the potential range for ICT counts by applying minimum and maximum values of gain for minimum and maximum ICT temperatures to compute the range of variability for the difference (ICT-SP) in Eq (1). Minimum and maximum gains are determined from analysis of multiyear data, similar to the one presented in Fig. 6. The relative variations of gain and offset within one orbit are typically less than $\pm 5\%$, that is, 10% total. For the HRPT scene we assume limits of $\pm 3\%$. Since SP count is already defined earlier, we can determine the range of variability for ICT data as well. Thus established thresholds are applied to mark outliers in the ICT and (ICT-SP) datasets, which fall outside of predetermined limits. Suspicious data are then replaced by linear interpolation between two good neighboring points. An example of data for channel 3 on 1 December 1988 is given in Fig. 7 for *NOAA-11*. Upper and lower envelope curves, computed as 5% limits around the average data, determine the cutoff limits. A strong effect of the solar blackbody contamination in the middle of the interval is observed.

c. Fourier transform filtering

The above robust procedures remove very efficiently many short-time noise fluctuations, especially single transmission errors. Nevertheless, the errors occurring over long-time intervals may still persist. To further reduce the effect of outliers that may exist within the potential range of variability, as well as to provide some smoothing and reduce noise in the data, we apply a Fourier transform filter. This filtering removes the harmonics with a period of less than 1 min, equivalent to 360 scan lines of HRPT data and 120 scan lines of GAC data. For PRT data, a 1-min period covers 72 cycles for HRPT data and 24 cycles for GAC data, respectively. The selection of a 1-min interval is based on power spectrum analysis. Examples of power spectra are given in Fig. 8 for PRT and ICT signals. Each power spectrum was normalized to unity for a harmonic with period equal to the orbital period. Plots show that the power spectra are reduced by a factor of $\sim 10^3$ for a 10-min component, and by a factor of $\sim 10^5$ for a 1-min component. A few harmonics with long periods ($>$20 min) account for most changes in the signal, while all remaining components have amplitudes below 1%.

Why do we need to combine the robust statistical technique and Fourier filtering to remove outliers in the calibration data? They complement each other. The robust approach is efficient in removing random isolated transmission errors, but not errors that last more than

the chosen sampling interval (12.5 s). Fourier filtering suppresses effectively any noise of low amplitude, but is quite helpless to remove outliers of large amplitude. This justifies the bounding of the calibration signal within certain limits.

Low-amplitude noise typically leads to increased contribution of high-frequency harmonics (Press et al. 1996). However, the strong short-term large amplitude distortion of the signal e.g., due to transmission error or loss of hardware synchronization) causes additive change in the power spectrum for the entire range of frequencies. This is illustrated by the decomposition of Dirac's δ-function

$$\delta(x) = \frac{1}{2\pi} \int_{-\infty}^{+\infty} e^{ikx}\, dk, \qquad (7)$$

where all Fourier harmonics over infinite interval of wavenumbers k have constant amplitude ($1/2\pi$). An example of the influence of a large single outlier on Fourier filter smoothing is presented in Fig. 9. Figure 9 shows a typical PRT signal disturbed by a single large outlier of maximum amplitude, like that one presented in Fig. 2b. Fourier transform filtering shown in Fig. 9a certainly reduces its magnitude, although the distortion is still quite large. In fact it even exceeds the apparent maximum value of the true signal. When an outlier is bounded by limiting value, as described above, the same filtering removes the outlier almost perfectly.

A more detailed example of the application of Fourier transform filter is given in Fig. 10. We analyze the same data as presented in Fig. 5, except SP data for channel 4, which do not require any further refinement. Plots on the left side of Fig. 10 are similar to Fig. 5 except they show smoothed curves obtained by a Fourier filter instead of robust results. The right panels present the distribution of deviations between Fourier smoothed curve and robust results, as well as between the Fourier smoothed curve and results obtained by standard averaging method. The superior results obtained by the robust method over the simple averaging approach are evident. For example, the number of outliers with $|\Delta C| \geq 2$ shown in Figs. 10b,d after the robust procedure has been reduced substantially: from 52 (b) and 70 (d) to 2 and 14, correspondingly. Outliers with large deviations were eliminated completely.

The data distribution analysis also enables us to propose a method for determining quality flags for calibration scans. When the deviation between the results of Fourier filtering and signal exceed some threshold value (chosen equal to two counts in the above example), then the data may be flagged as corrupted and replaced by linear interpolation between two good neighboring data points. Filtering then may be repeated iteratively until convergence (no further improvement) is achieved.

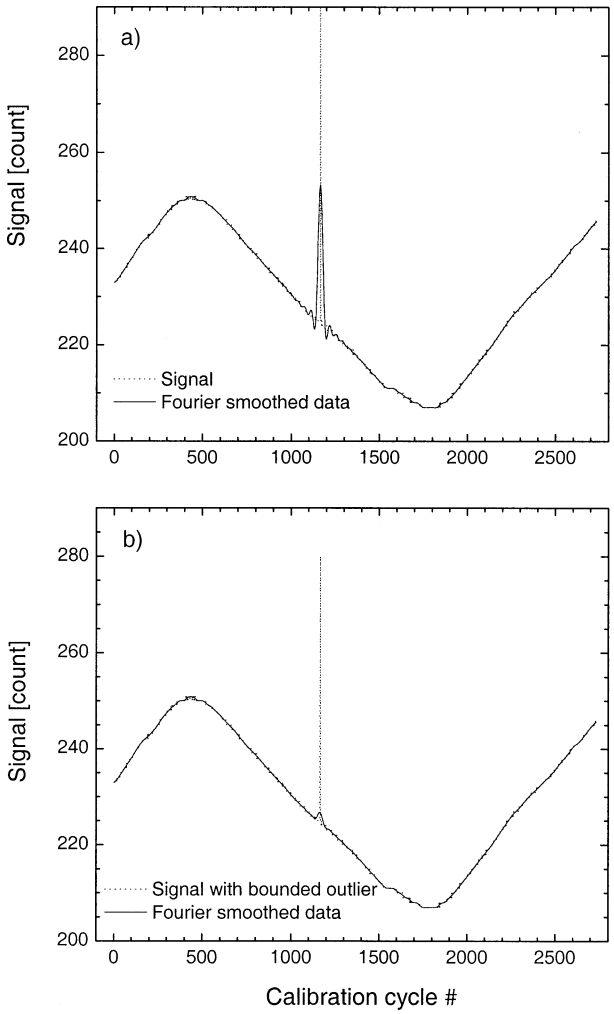

FIG. 9. Fourier transform filtering for (a) unbounded and (b) bounded outliers. Bounded outliers are corrected much more accurately than unbounded outliers with large amplitudes.

5. Removing unwanted fluctuations in gain and offset

The accuracy of thermal calibration required for climate monitoring and weather forecasting is estimated to be around ± 0.1 K (Kidwell 1998; Vazquez-Cuervo and Sumagaysay 2001). This demands high accuracy in the determination of instrument calibration coefficients. Procedures described in previous sections can remove high-frequency noise contamination and large outliers in the calibration measurements. Nevertheless, they are powerless in correcting fluctuations of gain and offset due to solar radiative contamination, which is quite ubiquitous phenomenon for AVHRR. It occurs on every orbit for all AVHRR instruments onboard NOAA satellites, including AVHRR *NOAA-16*. Removing this type of contamination is difficult due to its ''signal-like'' behavior.

Solar radiative contamination rapidly changes the

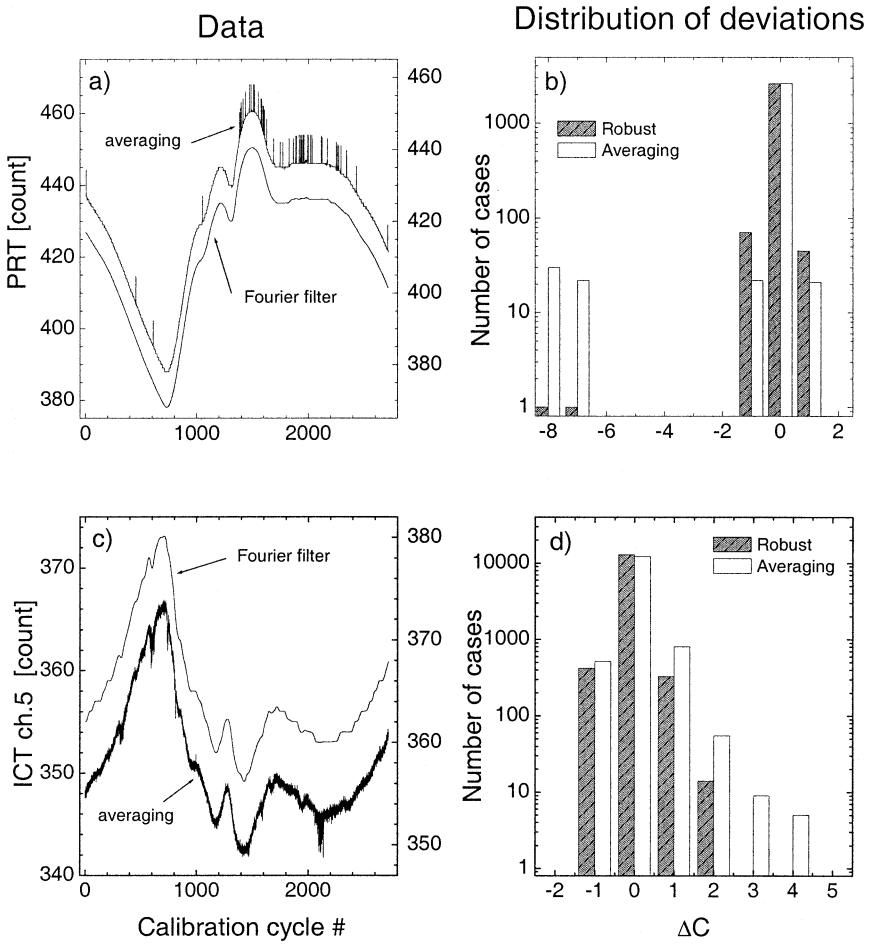

FIG. 10. (left) Application of Fourier transform filtering to (a) PRT and (c) ICT counts. (right) The distribution of deviations between Fourier filtering and robust and average estimation results for (b) PRT and (d) ICT data.

thermal state of the ICT radiating surface (Trishchenko and Li 2001a). The thermal inertia of PRT sensors implanted into the ICT does not allow tracking of these changes instantly. The PRT-determined ICT temperature is underestimated during heating periods and may be overestimated when the ICT surface cools down. This leads to a mismatch between computed and measured radiation in Eq. (1), which introduces a bias in the computed gain and offset. NOAA attempted to correct the effect of solar contamination in channel 3B (Kidwell 1998). NOAA's approach is based on a threshold technique that detects solar contamination events and replaces the gain and offset in channel 3B by constant values during these periods. No correction was applied to channel 4 and 5 gains.

Figure 11 demonstrates the importance of solar contamination for all thermal channels. Since the AVHRR detector system is designed to provide stability of the AVHRR measurement properties, we can consider short-term variations in gain and offset during solar contamination periods as artefacts. For example, the entire AVHRR detector system is maintained by a radiant coolant subsystem at a constant temperature around 107 K (Cracknell 1997). The large thermal inertia of the AVHRR components is also a factor. According to Walton et al. (1998), they have a long response time for thermal relaxation, ranging from 30 min to several hours. All these factors prevent significant short-term changes in the measurement properties of the AVHRR system. An effective way to eliminate these variations is the Fourier transform filtering technique similar to the one we introduced for the calibration measurements, but with longer cutoff periods (Trishchenko and Li 2001a). The length of the cutoff period depends on the duration of the solar contamination period. We estimate that a 10 to 15-min cutoff limit is adequate for filtering of solar contamination effects in the gain time series. The duration varies with time due to the satellite orbit precession and depends on the angle between the sun and satellite orbital plane. Filtering must be applied for all thermal channels.

Figure 11 shows the results derived by applying a

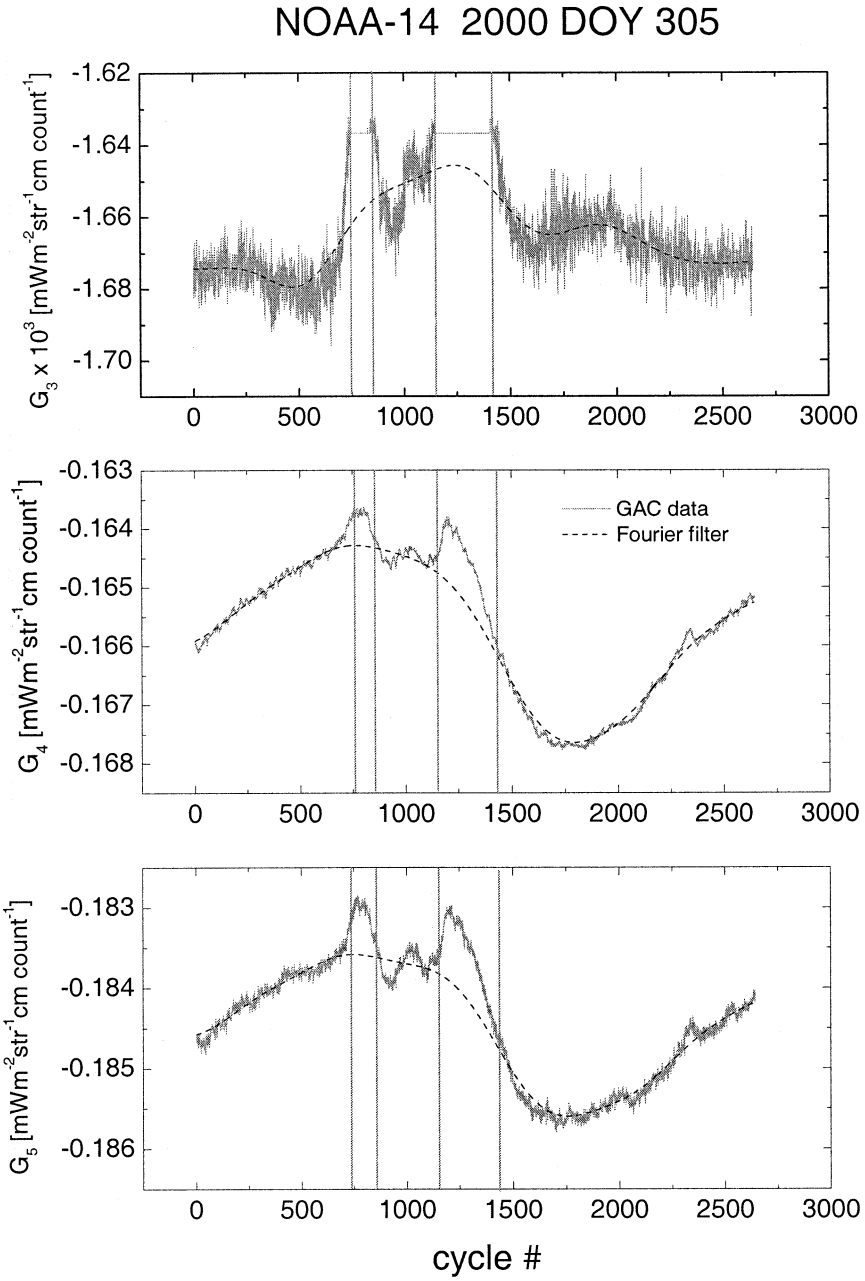

FIG. 11. Removing solar radiative contamination effect in AVHRR gains for (a) channel 3, (b) channel 4, and (c) channel 5. GAC data for AVHRR *NOAA-14* on 1 Nov 2000.

Fourier transform filter with a 10-min cutoff limit. Vertical lines denote intervals when channel 3B gain was corrected due to solar contamination as determined by corresponding flags in the NOAA GAC data. One can see that the Fourier filtering provides a good approximation for gain outside of solar contamination periods and allows us to correct spikes caused by solar contamination. Channel 3B data shown in Fig. 11 include some correction as implemented in the GAC data processing. Clearly, the substitution of a constant value for the gain is not the best choice.

The effect of solar contamination in terms of ICT temperature error is presented in Fig. 12. This figure shows the difference between PRT-derived temperature and the temperature reconstructed from the corrected gain. Results are plotted versus the latitude of spacecraft position. Filtered and original GAC data are within ± 0.1 K on the part of the orbit where no solar contamination of calibration data occurs. Solar contamination in Fig. 12 biases temperature up to 0.5 K. Analysis revealed that for historical data, such as *NOAA-9* to *-12*, the correction may approach the magnitude $\sim$1 K (Trish-

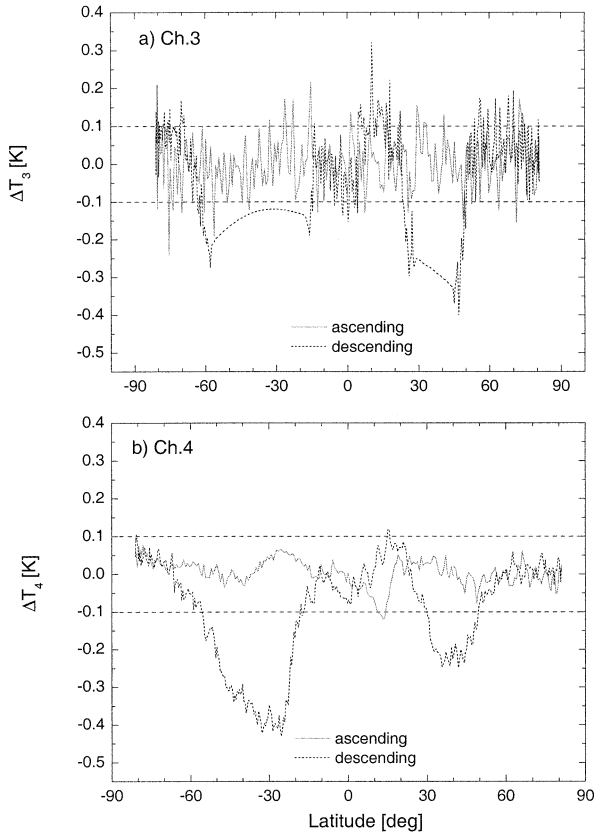

FIG. 12. Effect of solar contamination on the determination of pixel brightness temperature. Errors were computed for true pixel brightness temperature equal to ICT temperature (~290 K). Results are for (top) channel 3 and (bottom) channel 4. Channel 5 is similar to channel 4. Results for ascending and descending parts of the orbit are shown as solid and dashed lines.

chenko and Li 2001a). Corrected to constant levels, the channel 3 calibration still noticeably biases the brightness temperature in this channel. Undercorrection as shown in Fig. 12a may be as high as 0.4 K. For parts of the orbit with unperturbed calibration our method provides results within acceptable range of uncertainty 0.1 K.

6. Time-dependent versus scene average calibration for HRPT data

a. Effect of gain variation

Often, the thermal calibration of the AVHRR HRPT data employs scene average gain and offset parameters. This approach, for example, is accepted in GEOCOMP-N data processing at CCRS. Examples of the AVHRR calibration data presented earlier show that calibration coefficients are time dependent. How does this variation affect the accuracy of calibrated data in terms of brightness temperature?

The magnitude of the effect depends on the amplitude

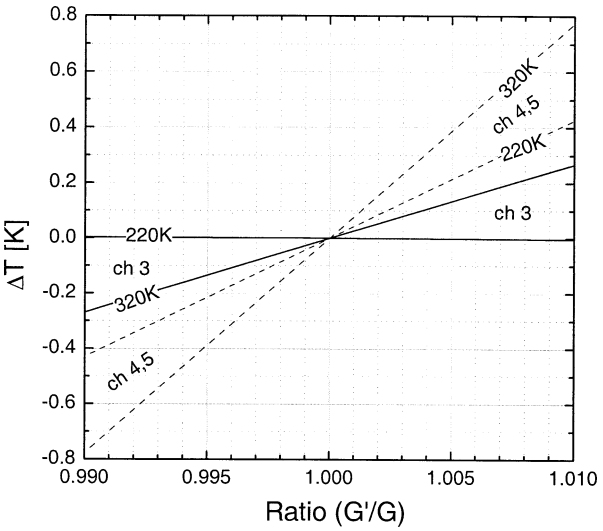

FIG. 13. Errors in brightness temperature due to uncertainty in channel gain. Errors are shown as the area limited by 220- and 320-K lines, which corresponds to true pixel brightness temperature. Areas for channel 3 (solid lines) and channels 4, 5 (dashed lines) are shown. Results were computed using gains from Table 2.

of instrument gain variation. Equation (1) yields the following expression for pixel linear radiance $R_p^{(i)}$

$$R_p^{(i)} = G^{(i)}(C_p^{(i)} - C_{\mathrm{SP}}^{(i)}) + R_{\mathrm{SP}}^{(i)}. \tag{8}$$

As we have shown earlier, the space count $C_{\mathrm{SP}}^{(i)}$ is a nearly constant quantity. The deep-space equivalent radiance $R_{\mathrm{SP}}^{(i)}$ is assigned a constant value. Therefore, the only factor that really determines the accuracy of pixel radiation is the uncertainty in channel gain $G^{(i)}$. One can easily derive the following expression for uncertainty in pixel radiation

$$\Delta R = R' - R = (G'/G - 1)R - R_{\mathrm{SP}}(G'/G - 1)$$
$$= (G'/G - 1)(R - R_{\mathrm{SP}}), \tag{9}$$

where R' is pixel radiance affected by an incorrect value of gain G'. Index (i) denoting channel selection was omitted in Eq. (9). We also neglected the nonlinear radiance correction, since it has an insignificant effect when the ratio G'/G is close to 1.

The relative error is determined by

$$\Delta R/R = (G'/G - 1)(1 - R_{\mathrm{SP}}/R). \tag{10}$$

Figure 13 shows typical results. They were computed based on calibration data presented in Table 1 and magnitude of gains for AVHRR *NOAA-14* and *-16* given in Table 2. Data in Table 2 represent the typical gains close to median values over the instrument lifetime periods. The results in Fig. 13 are plotted as intervals between two curves, corresponding to 220 and 320 K pixel brightness temperatures. Two sets of curves are for channel 3B and channels 4 and 5. Results were plotted as error in pixel brightness temperature versus ratio of affected gain to true gain. Variations in gain shown in

TABLE 2. Typical gains for the AVHRR thermal channels.

Channel	AVHRR/*NOAA-14* (mW m^{-2} str^{-1} cm count^{-1})	AVHRR/*NOAA-16* (mW m^{-2} str^{-1} cm count^{-1})
3B	−0.0016462	−0.002465
4	−0.16408	−0.18246
5	−0.18242	−0.19629

Fig. 13 are limited to ±1% around the true value (ratio = 1). Channels 4 and 5 are 2–3 times more sensitive to uncertainty in gain than channel 3B. The ±1% uncertainty in gain may lead to the error of ±0.4–0.8 K depending on brightness temperatures in channel 4 and 5. Corresponding error for channel 3B is within ±0.3 K. To achieve an accuracy ±0.1 K for channels 4 and 5 in the range of SST ($t > 0$°C), we have to determine the gain for these channels with an accuracy better than ±(0.1%–0.2%).

Impact of temporal variation in gain on brightness temperature is presented in Fig. 14 for two HRPT scenes acquired at PASS from AVHRR/*NOAA-14* on 1 July 1995 and 15 December 2000. Figure shows the differences between pixel brightness temperatures computed with scene average gains and time-dependent gains. Smoothed results are plotted. The true pixel brightness temperature was assumed equal to the scene average ICT temperature. The dashed curves represent results for 1 July 1995. Solid curves correspond to data for 15 December 2000. Temperature differences for July 1995 are within ±0.1 K for all channels, though unsmoothed data for channel 3B are noisy and the error may be as high as ±0.2–0.3 K (not shown). The dashed curve corresponds to the beginning of instrument and satellite operations. With time, spacecraft and instruments performance and stability may degrade, that leads to larger variations in calibration parameters (Trishchenko and Li 2001b). Drift of satellite orbit may also be a factor contributing to larger variability at the end of radiometer's lifetime. As such, similar errors for AVHRR/*NOAA-14* in the end of 2000 (solid curves) reach ±0.3 K for channels 4 and 5 and up to ±0.5 K for channel 3. There are also quite significant seasonal variations in the instrument thermal state (Fig. 6) that induce additional variations in the calibration data.

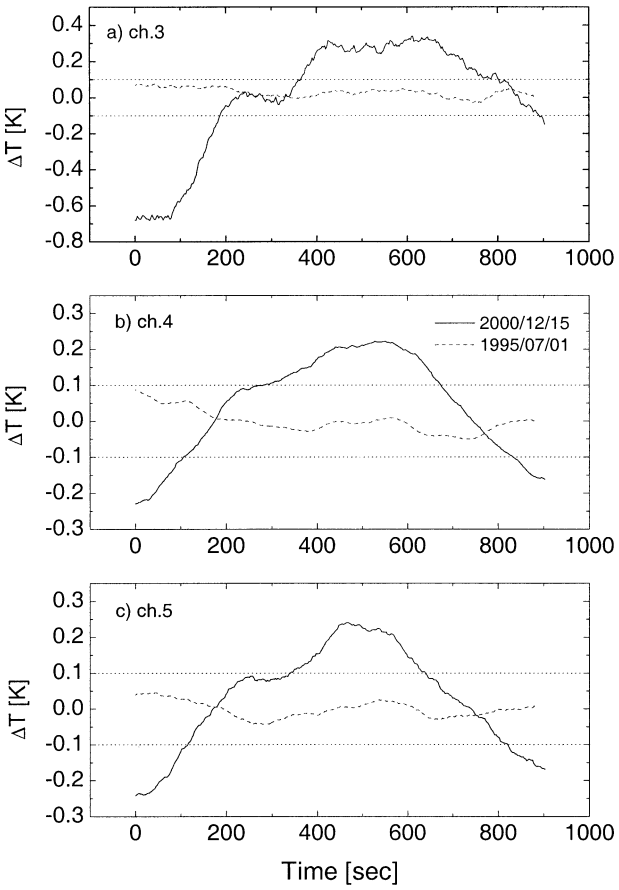

FIG. 14. Difference between pixel brightness temperatures determined with HRPT scene average and time-dependent gains. Results are for (a) channels 3, (b) 4, and (c) 5 of AVHRR/*NOAA-14*. Dashed lines depict data for 1 Jul 1995; solid curves are for 15 Dec 2000. Significant degradation of the stability of gains within HRPT scenes is observed since 1995. The interval of brightness temperature ±0.1 K is marked by dotted lines.

b. Effect of solar contamination on HRPT data

GAC data indicate, that solar contamination causes a large perturbation in the calibration system, and affects the accuracy of thermal data. The method we proposed for correcting this effect can be successfully applied to GAC data, which cover quite a long interval of time of up to 100 min or more. However, it cannot be applied for short scenes such as the HRPT images. The duration of these scenes (∼15 min) is approximately equal to the filtering cutoff period (10–15 min).

To correct the effect of solar contamination within a HRPT scene using Fourier transform filtering, joint analysis of HRPT and GAC data is required. This complicates real-time HRPT data processing quite significantly. Nevertheless, this seems a necessary step to provide better accuracy of thermal calibration for short scenes affected by solar contamination. It is possible that a significant portion of or even an entire HRPT scene may be contaminated. Solar contamination cannot be corrected in this case due to limited information about the unperturbed calibration signal.

We suggest two ways to overcome this problem. First, one can use a typical ''latitudinal model'' for channel gains. This model captures the variation of gains depending on the latitude of the subsatellite point. Since the satellite motion is periodic, the calibration performance repeats quite closely during several orbits. HRPT data processing using a latitudinal model also can be done in real-time mode, since the model can be derived in advance based on previous GAC data. The GAC data can be accessed from the NOAA SAA. An example of the latitudinal model is presented in Fig. 15 for AVHRR/

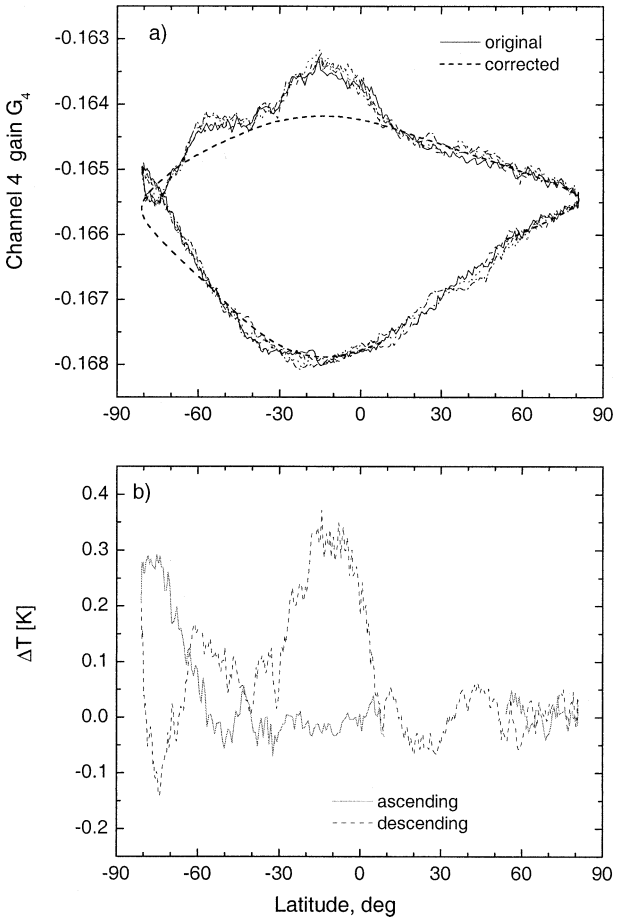

FIG. 15. Variation in gain with satellite latitude (latitudinal model). (a) AVHRR/*NOAA-14* channel 4 gain is shown for five consecutive orbits. The dashed line depicts the gain corrected for the solar radiative contamination according to method proposed in this paper. (b) shows the difference in brightness temperature derived with original and corrected gains. Data are for 1 Apr 2000. Results for ascending and descending parts of the orbit are shown as solid and dashed lines on bottom panel.

NOAA-14. Figure 15a shows the gain of channel 4 for five consecutive orbits. Data for all orbits follow each other very closely. The dashed curve depicts the gain corrected for solar contamination as proposed above. Figure 15b shows the error in ICT temperature computed from the difference between uncorrected and corrected gains. Uncorrected gain causes errors up to ± 0.4 K. As mentioned above, this bias occurs due to solar blackbody contamination and the thermal inertia of PRT sensors used to measure the ICT temperature (Trishchenko and Li 2001a; Cao et al. 2001).

More accurate HRPT data processing can be achieved with a ''temporal model'' that uses time-dependent calibration coefficients derived from GAC data. However, real-time data processing is not possible with this approach unless HRPT and GAC data are processed together in real time.

7. Conclusions

Increasing concerns about current climate change dictate high demands on the accuracy of quantitative monitoring of the thermal regime of the planet. Modern weather forecasting is putting forward similar demands. Satellite information is the only plausible tool to reach this goal. Thermal measurements available from AVHRR onboard of the NOAA polar-orbiting satellite are an important component of a global weather and climate-observing system. AVHRR provides information about the SST field, thermal state of the earth's surface and cloud cover. Despite a long history of the AVHRR observations, the accuracy of these measurements remains largely undetermined. This study attempted to shed more light on this subject.

Detailed analysis of the nature and consequences of various fluctuations in the AVHRR thermal calibration data has been conducted. We analyzed two types of data: 1) HRPT data and 2) GAC data. The HRPT data were acquired from Prince Albert Satellite Station, which is the major AVHRR reception facility for Canada Centre for Remote Sensing. The AVHRR GAC data were acquired from the NOAA Satellite Active Archive. It was shown that typically between 1% and 2% of HRPT monthly scenes processed at CCRS by GEOCOMP-N system are affected by large outliers in the calibration data. Outliers in the data may arise during transmission and decoding of radio signal, as well due to noise generated as a result of various internal processes in the AVHRR radiometer. Special attention must be paid to the effects caused by solar radiative contamination. This effect produces large amplitude signal-like perturbation (bias) of calibration gain and offset.

Novel methods of quality control and robust calibration are proposed. They are superior in removing unwanted fluctuation in the calibration data relative to commonly used techniques based on an averaging approach. The proposed method combines three steps: 1) robust estimation of ICT, SP calibration measurements, and PRT counts based on a modified median filter, 2) limiting large amplitude outliers within prescribed bounds based on the robust criteria and physical principles, 3) Fourier transform filtering of short-term variations in the calibration data with periods less than 1 min.

It is confirmed that the solar contamination is a common phenomenon for all AVHRR instruments, including AVHRR/3 onboard *NOAA-16*. It occurs on the certain parts of the satellite orbits, when the sun light impinges on the AVHRR interior, and causes contamination in all thermal channels. Biases in pixel brightness temperature due to solar contamination typically are around 0.5 K and may reach a magnitude close to 1 K. The thermal contamination effect occurs due to heating as result of absorption of solar radiation by the AVHRR ICT and radiometer interior. This heating leads to an imbalance between PRT readings and effective temperature of the

ICT thermal radiation. This causes unwanted spurious fluctuations in calibration gain and offset. We propose a method for removing this fluctuation in GAC data by Fourier transform filtering of the channel gains and cutting off all harmonics with periods equal to or shorter than the period of solar contamination (10–15 min). Method works more effectively when Fourier filtering is applied iteratively. Convergence is usually achieved after 2–3 iterations.

Some opportunities were also discussed to correct the solar contamination in the HRPT data, when a significant portion of or even an entire HRPT scene may be contaminated. Two solutions were proposed: latitudinal model and temporal model. Both approaches require a joint analysis of the HRPT and GAC data. Methods proposed in the paper may be useful for the development of calibration techniques for similar radiometers and future National Polar-Orbiting Operational Environmental Satellite System sensors.

Acknowledgments. The author is very grateful to Gunar Fedosejevs (CCRS) for valuable comments and careful reading of the manuscript. Thanks are also due to William Park (CCRS) for technical assistance with HRPT data handling. The use of AVHRR GAC data acquired through the NOAA SAA is gratefully acknowledged.

REFERENCES

Adair, M., J. Cihlar, B. Park, G. Fedosejevs, A. Erickson, R. Keeping, D. Stanley, and P. Hurlburt, 2002: GeoComp-n, an advanced system for generating products from coarse- and medium-resolution optical satellite data. Part 1: System characterization. *Can. J. Remote Sens.,* **28,** 1–20.

Alexejev, M. I., A. N. Andrievsky, N. A. Zaitsev, and A. P. Trishchenko, 1994: Investigation of data reception quality for the satellites METEOR (in Russian). *Meteor. Gidrol.,* **N5,** 32–35.

Barnett, V., and T. Lewis, 1994: *Outliers in Statistical Data.* Wiley, 584 pp.

Cao, C., M. Weinreb, and J. Sullivan, 2001: Solar contamination effects on the infrared channels of the Advanced Very High Resolution Radiometer (AVHRR). *J. Geophys. Res.,* **D106,** 33 463–33 469.

Cihlar, J., J. M. Chen, Z. Li, F. Huang, R. Latifovic, and R. Dixon, 1998: Can interannual land surface signal be discerned in composite AVHRR data? *J. Geophys. Res.,* **103,** 23 163–23 172.

——, and Coauthors, 2002a: GeoComp-n, an advanced system for the processing of coarse and medium resolution satellite data. Part 2: Biophysical products for northern ecosystems. *Can. J. Remote Sens.,* **28,** 21–44.

——, R. Latifovic, J. Chen, A. Trishchenko, Y. Du, G. Fedosejevs, and B. Guindon, 2002b: Systematic corrections of AVHRR image composites for temporal studies. *Remote Sens. Environ.,* in press.

Cracknell, A. P., 1997: *The Advanced Very High Resolution Radiometer (AVHRR).* Taylor and Francis, 534 pp.

Eskridge, R. E., O. A. Alduchov, I. V. Chernykh, Z. Panmao, A. C. Polansky, and S. R. Doty, 1995: A comprehensive aerological reference data set (CARDS): Rough and systematic errors. *Bull. Amer. Meteor. Soc.,* **76,** 1759–1775.

Goodrum, G., K. B. Kidwell, and W. Winston, cite 2000: NOAA KLM user's guide. U.S. Department of Commerce, NESDIS, NOAA, National Climatic Data Center, Satellite Data Services Division, Suitland, Maryland. [Available online at http://www2.ncdc.noaa.gov/docs/klm/cover.htm.]

Gutman, G., 1999: On the use of long-term global data of land reflectances and vegetation indices derived from the advanced very high resolution radiometer. *J. Geophys. Res.,* **104,** 6241–6255.

Houghton, A., 2001: *Error Coding for Engineers.* Kluwer Academic, 256 pp.

Kidwell, K. B., Ed.,1998: NOAA polar orbiter data user's guide. U.S. Department of Commerce, NESDIS, NOAA, National Climatic Data Center, Satellite Data Services Division, Washington, D.C.

Martin, R. D., 1981: Robust methods for time series. *Applied Time Series Analysis II,* D. F. Findley, Ed., Academic Press, 683–759.

Peterson, T. C., A. N. Basist, C. N. Williams, and N. C. Grody, 2000: A blended satellite–in situ near-global surface temperature dataset. *Bull. Amer. Meteor. Soc.,* **81,** 2157–2164.

Press, W. H., S. A. Teukolsky, W. T. Vetterling, and B. P. Flannery, 1996: *Numerical Recipes in Fortran 77: The Art of Scientific Computing.* 2d ed. Cambridge University Press, 1486 pp.

Reynolds, R. W., and T. M. Smith, 1994: Improved global sea surface temperature analyses using optimum interplation. *J. Climate,* **7,** 929–948.

Rousseeuw, P. J., and A. M. Leroy, 1987: *Robust Regression and Outlier Detection.* Wiley, 352 pp.

Sullivan, J., 1999: New radiance-based method for AVHRR thermal channel nonlinearity corrections. *Int. J. Remote Sens.,* **20,** 3493–3501.

Steyn-Ross, D. A., M. L. Steyn-Ross, and S. Clift, 1992: Radiance calibration of Advanced Very High Resolution Radiometer infrared channels. *J. Geophys. Res.,* **97,** 5551–5568.

Trishchenko, A. P., and Z. Li, 2001a: A method for the correction of AVHRR onboard IR calibration in the event of short-term radiative contamination. *Int. J. Remote Sens.,* **22,** 3619–3624.

——, and ——, 2001b: Internal consistency, consequences of solar blackbody contamination and temporal trends in the calibration of AVHRR's thermal channels. *Proc. IAMAS 2001,* Innsbruck, Austria, International Association of Meteorology and Atmospheric Sciences, 59.

Vazquez-Cuervo, J., and R. Sumagaysay, 2001: A comparison between sea surface temperatures as derived from the European remote sensing Along-Track Scanning Radiometer and the NOAA/NASA AVHRR ocean Pathfinder dataset. *Bull. Amer. Meteor. Soc.,* **82,** 925–944.

Viterbi, A. J., and J. K. Omura, 1979: *Principles of Digital Communication and Coding.* McGraw-Hill, 560 pp.

Walton, C. C., J. T. Sullivan, C. R. N. Rao, and M. P. Weinreb, 1998: Corrections for detector nonlinearities and calibration inconsistencies of the infrared channels of the Advanced Very High Resolution Radiometer. *J. Geophys. Res.,* **103,** 3323–3337.